A COMPARISON OF A THREE PHASE INDUCTION MOTOR FED BY TWO DIFFERENT VOLTAGE SOURCES BEHAVIOR

Aurel-Ionuț CHIRILĂ[1], Ioan-Dragoş DEACONU[2], Constantin GHIȚĂ[3], Valentin NĂVRĂPESCU[4], Gianfranco CHICCO[5]

Maşinile asincrone sunt proiectate în general pentru o alimentare cu tensiuni sinusoidale. Dacă maşina este alimentată de la un invertor apar o serie de probleme care pot provoca deteriorarea acesteia în timp. Din acest motiv este importantă cunoaşterea fenomenelor ce apar în maşină. Modalitatea actuală de proiectare a maşinilor electrice implică şi generarea de prototipuri virtuale cu ajutorul diverselor programe de simulare. Lucrarea prezintă o comparaţie între comportamentul intern al unui motor asincron alimentat de la un sistem trifazat simetric sinusoidal de tensiuni respectiv de la un invertor de tensiune cu şase pulsuri.

In general induction machines are designed for sinusoidal voltages supply. When the machine is fed by an inverter a series of issues that can damage the machine arise. Thus, it is important to know the phenomena that are taking place inside the machine. At present induction machines' manufacturers use the advantage of different modeling and simulation software environments in order to create virtual prototypes. The paper presents a comparison between the internal behavior of a three-phase induction motor fed by sinusoidal voltages and by a six-pulse voltage inverter respectively.

Keywords: three-phase induction motor, six-pulse inverter model, finite element method.

1. Introduction

It is known that induction motors fed from inverters cause different stresses over the machine: audible noise due to resonance frequencies [1], increased losses and heat when low switching frequencies are used [2], insulation stress due to the short rising times of the supplying voltages that generate reflections [3 – 5], the bearings damages induced by circulating currents that are flowing through the capacitive couplings between the stator and the rotor [6]. For

[1] Assist., Electrical Engineering Fac., Universitatea POLITEHNICA Bucureşti, Romania
[2] Assist., Electrical Engineering Fac., Universitatea POLITEHNICA Bucureşti, Romania
[3] Prof., Electrical Engineering Fac., Universitatea POLITEHNICA Bucureşti, Romania
[4] Prof., Electrical Engineering Fac., Universitatea POLITEHNICA Bucureşti, Romania
[5] Prof., Department of Electrical Engineering, Politecnico di Torino, Italy

these reasons at present there are still studies regarding the internal phenomena based on simulations [7 – 13].

The electromagnetic field inside the induction motor can be used to determine its parameter variations [14]. For example in [15] based on the magnetic field the lumped parameters are determined and in [16] fictive identification tests have been carried out by the finite element method during the development and optimization process, without the necessity of cost-extensive prototyping.

In this paper, a co-simulation environment has been used in order to determine the behavior of a three-phase induction motor when it is fed by a six-pulse voltage inverter (see Fig. 1) and when it is fed by a sinusoidal three-phase symmetrical voltage system.

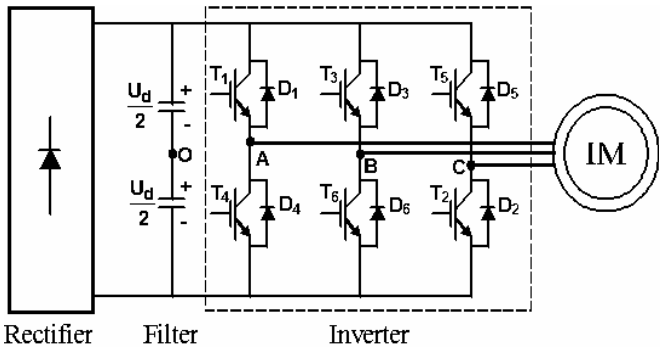

Fig. 1. Circuit diagram assembly (six-pulse voltage inverter and induction motor).

The motor that is modeled has been originally designed for sinusoidal voltages. Based on the simulation results, solutions on improving the design of induction motors when supplied from six-pulse voltage inverter (ways for diminishing the magnetically stressed zones inside the motor) may be purposed. A major advantage of such approach is that the induction machine's model behavior is similar to the real machine's behavior because non-linear materials' characteristics and specific phenomena such as skin effect for the rotor-bars currents are taken into account. The magnetic field inside the machine is calculated using the finite element method [17 – 18].

2. Co-simulation environment description

In order to obtain the magnetic field inside the induction motor when it is fed by sinusoidal voltages or by a six-pulse voltage inverter, two different software environments have been used. The models of the inverter and the sinusoidal three-phase symmetrical voltage system have been implemented using MATLAB/Simulink environment (developed by Mathworks [19]). The induction

motor's model has been designed using MagNet 6.26.1 software (developed by Infolytica [20]). In Fig. 2 the co-simulation model (induction motor and supply source) for the six-pulse voltage inverter is presented.

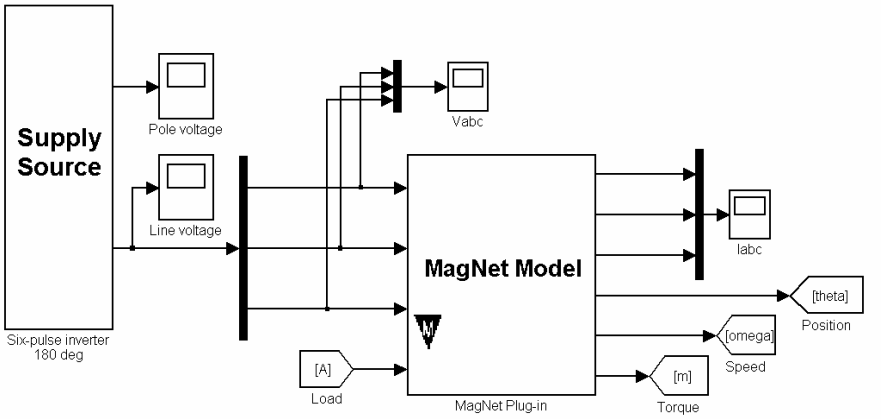

Fig. 2. Circuit diagram assembly (six-pulse voltage inverter and induction motor).

The same co-simulation model is used when the induction motor is fed by sinusoidal voltages but the inverter's block is replaced with three sinusoidal sources.

The inverter's MATLAB/Simulink model is shown in Fig. 3. Each arm of the inverter is controlled by a specific signal provided by ctrl1, ctrl2 and ctrl3 sources. These sources provide the control program of 180^{o} for the inverter. Based on the pole-voltages (uAO, uBO and uCO) the output line voltages are obtained, e.g. $uAB = uAO - uBO$.

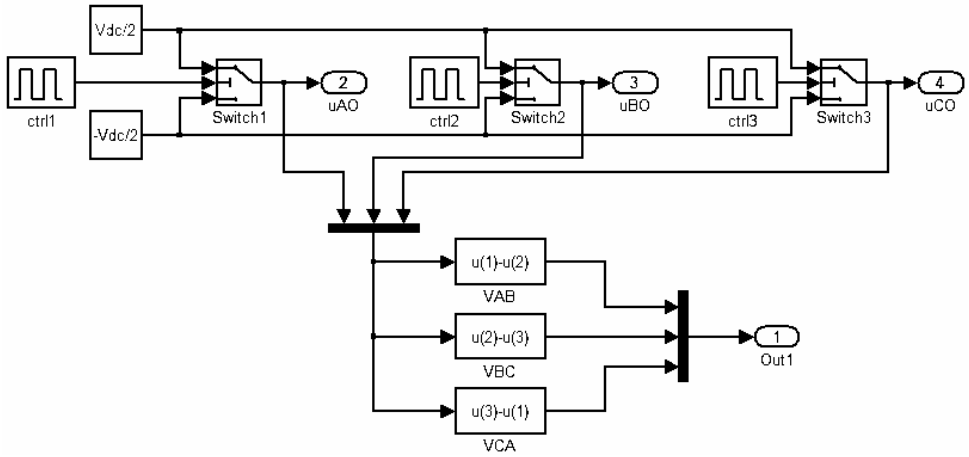

Fig. 3. Six-pulse MATLAB/Simulink inverter model.

This type of inverter has some advantages but some limitations also. The control is not so complex and the switching losses have low values because during one period of the output voltage's fundamental just two switching occur for each of the six semiconductor devices. Another advantage is the raised RMS value of the output line voltage fundamental [21]:

$$u_{AB}^{(1)} = \frac{\sqrt{6}}{\pi} U_d \tag{1}$$

where U_d is the inverter's DC input voltage supplied by the rectifier (see Fig. 1).

The drawback is that for inductive loads the resulting currents are not sinusoidal but in exchange have exponential variations.

A six-pulse voltage inverter can be obtained from a PWM voltage inverter by over modulation. The PWM inverter controls the output voltage by means of modulation factor while the six-pulse voltage inverter by means of the input DC voltage U_d.

The induction motor has the following rated data: power $P_{\mathrm{n}} = 0.125$ kW; voltage $U_{\mathrm{n}} = 380/220$ V ($\curlywedge$ / Δ); current $I_{\mathrm{n}} = 0.55/0.95$ A ($\curlywedge$ / Δ); speed $n_{\mathrm{n}} = 1380$ rpm.

Fig. 4 depicts the main geometrical dimension of the stator and the rotor respectively along with details on the stator and rotor slots. The air-gap of the machine is $\delta = 0.2$ mm.

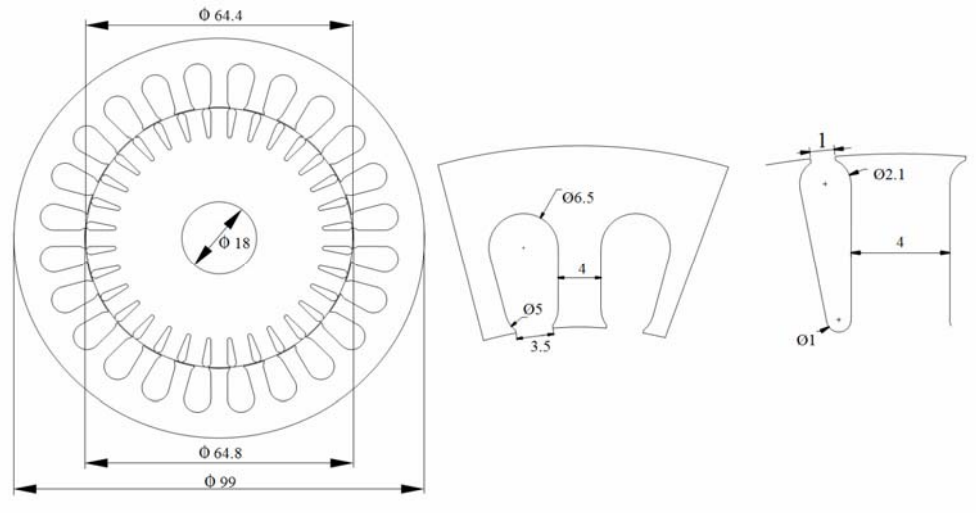

Fig. 4. The main geometrical dimensions of the stator and the rotor respectively.

Both stator and rotor teeth have parallel edges. Usually these types of teeth are used for induction motors that drive mono-block pumps.

Table 1 and Table 2 describe the features of the stator and rotor windings respectively.

Table 1

Stator winding

Quantity	Symbol	Value
Slots number	Z_1	24
Pair-poles	p	2
Slots per pole and phase	q_1	2
Phases	m_1	3
Coils pitch	y_1	5
Coils per phase	N_{cph1}	4
Layers	L_{w1}	3
Turns per phase	w_1	960

The stator winding diagram is presented in Fig. 5. Each phase is placed in its own layer, the coils have equal pitch and each slot has only one coil edge.

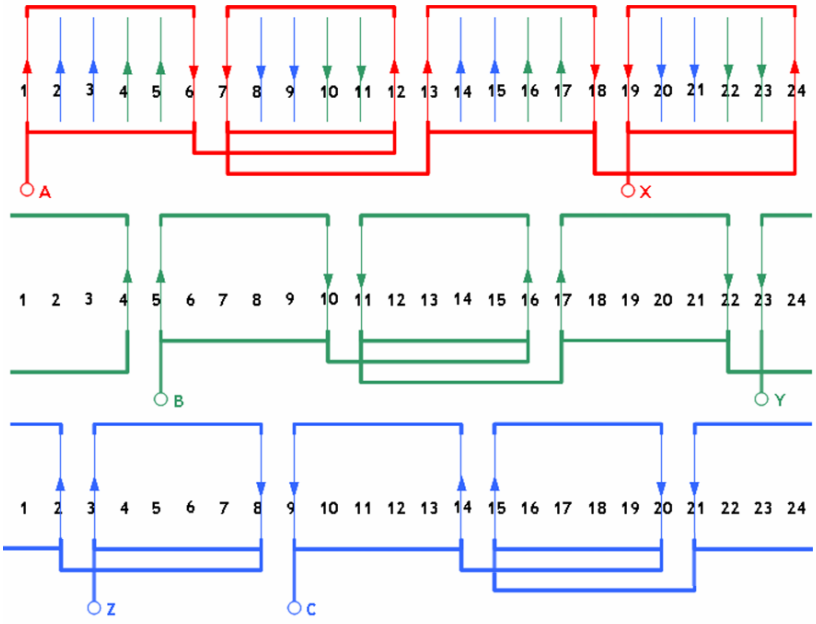

Fig. 5. The stator winding diagram.

Table 2

Rotor winding – squirrel cage

Quantity	Symbol	Value
Slots number	Z_2	36
Pair-poles	p	2
Slots per pole and phase	q_2	0.25
Phases	m_2	36
Coils pitch	y_2	1
Coils per phase	N_{cph2}	1
Turns per phase	w_2	0.5

The final model implemented in MagNet is presented in Fig. 6 with its components shown in perspective. The stator core and the rotor core have the same length $l_i = 41$ mm. The problem defined in MagNet is a 2D problem with plane-parallel symmetry.

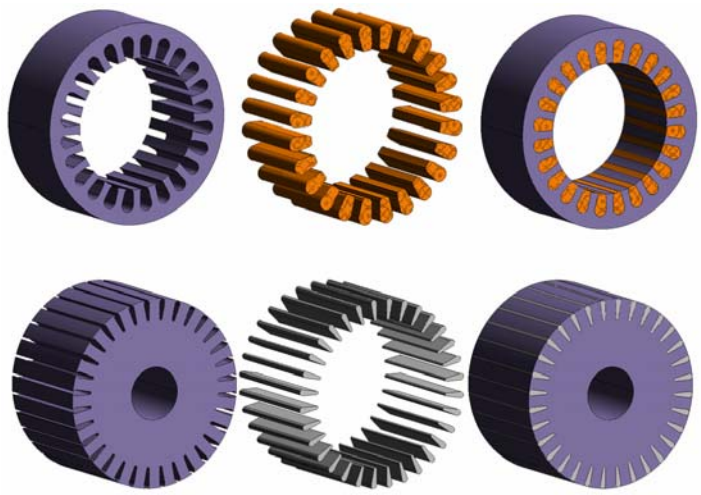

Fig. 6. Detailed motor model implemented in MagNet:(first line) stator core; stator winding; full stator;(second line) rotor core; rotor winding; full rotor.

The motor's electric circuit parts are also implemented in MagNet. Thus, in Fig. 7 and Fig. 8 the stator circuit and the rotor circuit respectively are presented. The stator windings are wye connected. Because the model is 2D the parameters *R_adit_i* and *Ls_frontend_i* (*i = {1, 2, 3}* see Fig. 7) replace the stator end-windings [22]. Each rotor bar is modeled by a coil and the rings' segments of the squirrel-cage have been replaced with resistances and inductances computed as in [22].

The supplying voltage sources wave-shapes (V1, V2 and V3) are controlled from MATLAB/Simulink environment.

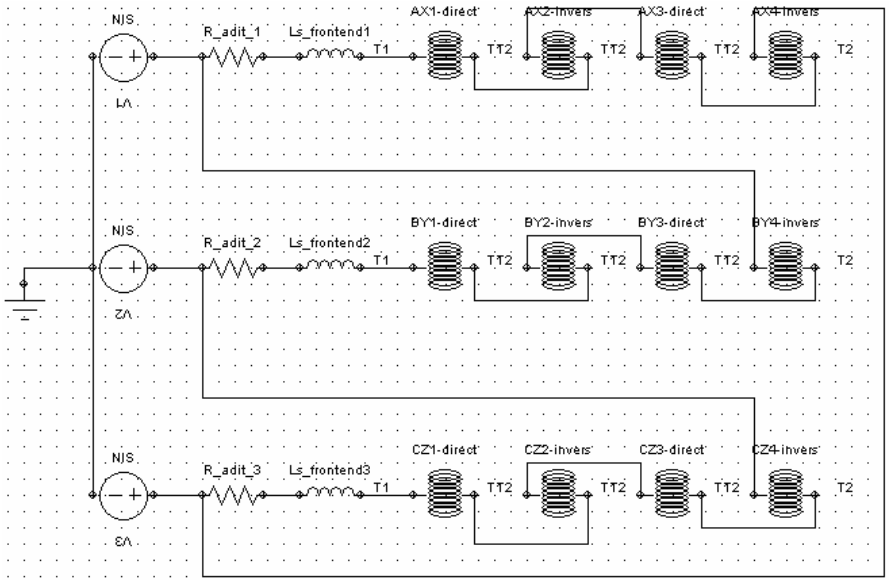

Fig. 7. Stator circuit and supplying voltage sources.

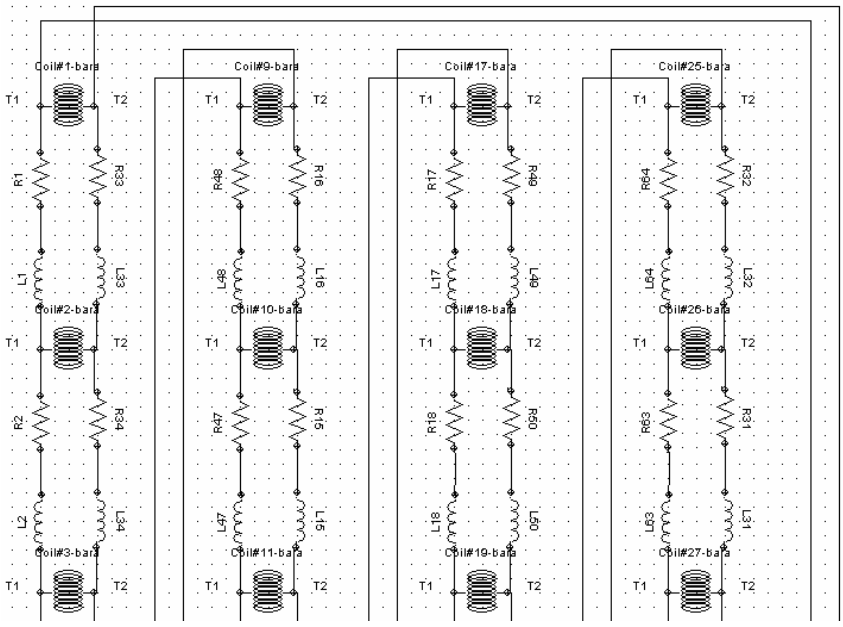

Fig. 8. Rotor circuit (squirrel-cage).

3. Magnetic field numerical computation method

The magnetic field problem resolved in this case is a 2D plane parallel problem with moving parts. The magnetic quantity that is solved for is the vector-potential $\vec{A}$ and electro-dynamic potential V [23].

$$\nabla \times \left(\nabla \times \vec{A}\right) \Big/ \mu + \sigma + \partial \vec{A} / \partial t - \left(\vec{v} \times \nabla \times \vec{A}\right) = -\sigma \cdot \nabla V \tag{2}$$

$$\vec{B} = \nabla \times \vec{A} \tag{3}$$

$$\vec{B} = \mu \cdot \vec{H} = \mu_0 \cdot \mu_\mathrm{r} \cdot \vec{H} \tag{4}$$

$$\nabla \times \vec{H} = \vec{J} \tag{5}$$

Equation (2) is the one solved by MagNet using finite element method where ∇V is given by the voltage sources. The solution is the magnetic vector-potential $\vec{A}$. The resulting magnetic flux density $\vec{B}$ yields immediately from (3) (i.e. magnetic flux density divergence is zero) and so is the magnetic field strength $\vec{H}$ using the material's law (4). The current densities $\vec{J}$ are obtained using Ampere's law (5) (where the displacement currents $\partial \vec{D} / \partial t$ were neglected because of the low frequency – $\omega \cdot \varepsilon / \sigma << 1$).

MagNet uses Galerkin finite element method based on hierarchical edge elements (Whitney elements) with triangular shape [20]. The solution in each element of the mesh is modeled as a linear superposition of n^{th}-order Lagrange polynomial base functions of the spatial coordinates (x, y). In this case first order polynomials have been selected.

Because the problem contains moving parts the mechanical equation of motion (6) is also solved for each simulation time step.

$$J \cdot \frac{d\Omega}{dt} = T_m - T_l \tag{6}$$

Mechanical effects include inertia and load torque (T_l that is specified by the user). The inertia moment (J) is automatically computed or is specified by the user. The electromagnetic torque is computed using the following formula:

$$T_m = \int_V \vec{r} \times \vec{f} \cdot dV \tag{7}$$

where $\vec{r}$ is a vector going from the model's origin to an element of volume in the body, V is the volume of the body and $\vec{f}$ is the force density (for this 2D problem $\vec{f}$ is obtained using the second Maxwell stress tensor [24]).

For each time step MagNet computes the magnetic field (2) and based upon it the electromagnetic torque (7). Using the specified load torque and (6) the net torque ($J \cdot d\Omega/dt$) yields. By integrating twice the angular acceleration over one time step the new rotor position is found. Thus the model's geometry is changed and remeshed. This solving algorithm is repeated for all the time steps.

4. Simulation results

In order to obtain the magnetic field inside the induction motor the co-simulation model (see Fig. 2) was used. The start-up transient regime of the motor has been analyzed using the numerical computation method described in section 3 (2D finite element method).

In the first case the motor is supplied with a sinusoidal three-phase symmetrical voltage system. In the second case the motor is supplied with six-pulse voltages. In both cases the rated load is applied ($T_l = 0.87$ Nm). In Fig. 9 one of the supplying line voltage, u_{AB} is represented for both cases.

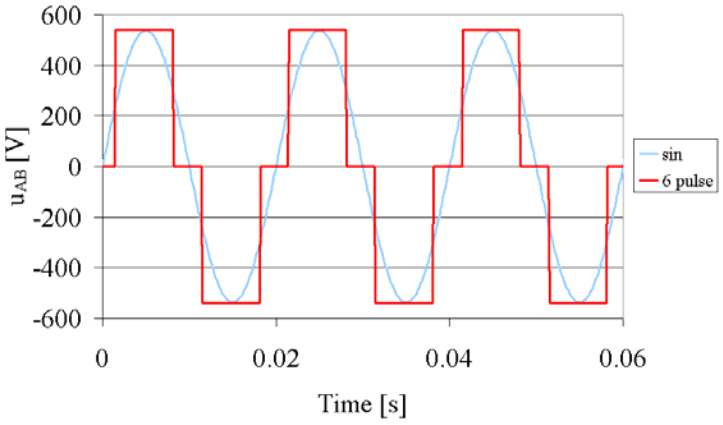

Fig. 9. Sinusoidal line voltage (blurred line) and six-pulse line voltage (thick line).

Fig. 10 depicts the line current i_A (because of the wye connected winding this is also the phase current). The current has a sinusoidal variation for the sinusoidal three-phase symmetrical voltage system while for the six-pulse voltage

the current is raising and falling after an exponential law. The exponential variation is in fact, the motor's response to a step voltage input signal, thus underlining its RL load type. One may see that the current corresponding to the six-pulse voltage case has a peak value greater than the current corresponding to the sinusoidal voltage case. This statement is also valid for the computed RMS values. Thus the induction motor has a greater acceleration for the six-pulse voltage case (see Fig. 11) [25].

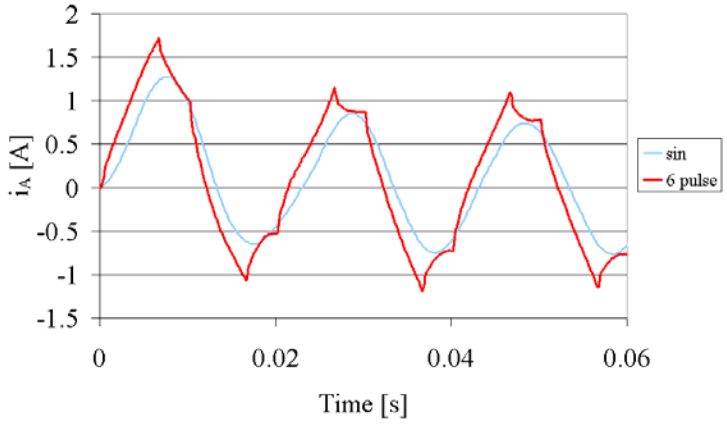

Fig. 10. Sinusoidal line current (blurred line) and six-pulse line current (thick line).

In order to compare the internal behavior of the three-phase induction motor fed by sinusoidal voltages and by a six-pulse voltage inverter respectively, the magnetic field inside the motor for the same mechanical rotor position was considered (see Fig. 12 and Fig. 13). The rotor's position was chosen after the induction motor has reached a steady-state regime ($t > 50$ ms).

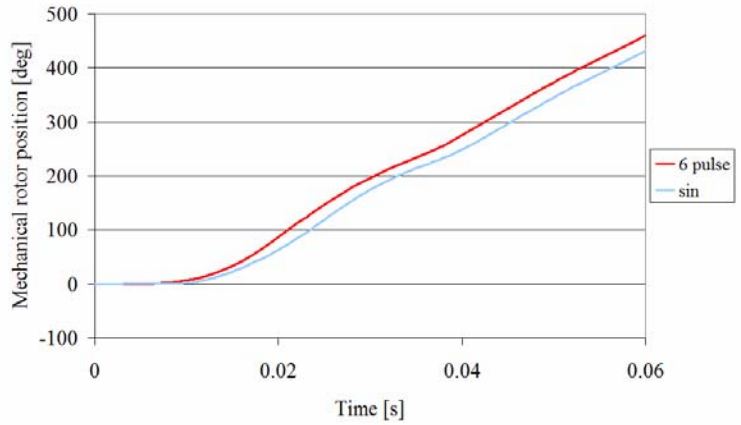

Fig. 11. The induction's motor mechanical rotor position for both cases.

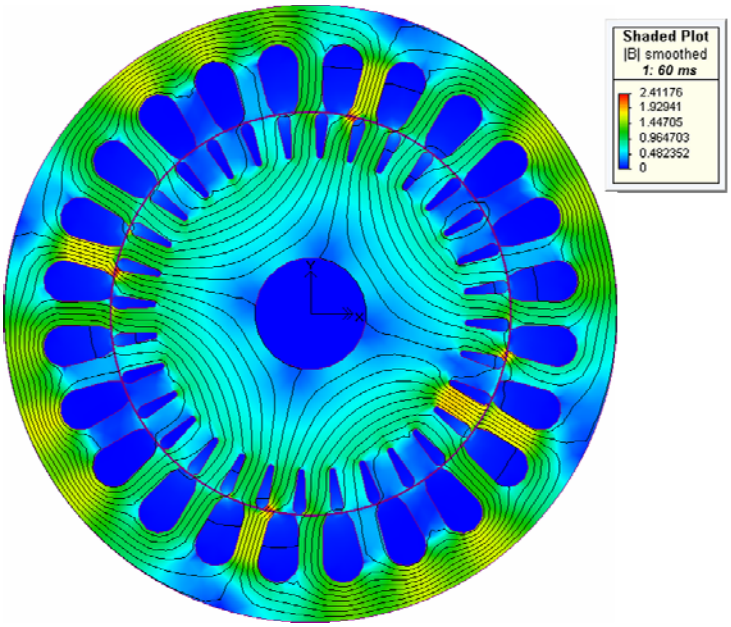

Fig. 12. Magnetic flux density map when the induction motor is fed by sinusoidal voltage.

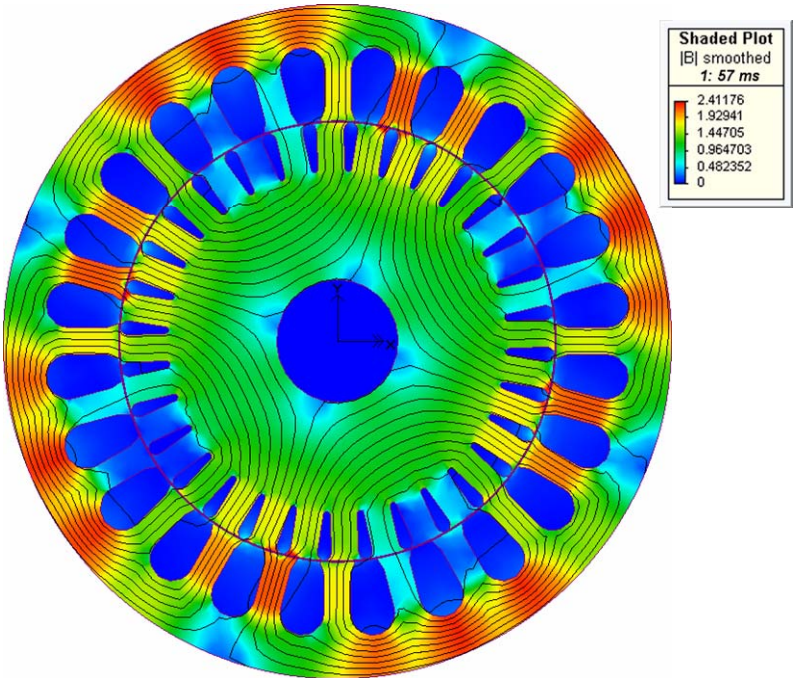

Fig. 13. Magnetic flux density map when the induction motor is fed by six-pulse voltage.

The time variation of the induction's motor mechanical rotor position for both cases is depicted in Fig. 11.

Fig. 12 and Fig. 13 show the magnetic flux density map (for the same mechanical rotor position) for a sinusoidal three-phase symmetrical voltage supply system ($t = 60$ ms – see Fig. 11) and for a six-pulse voltage supply system, respectively ($t = 57$ ms – see Fig. 11).

5. Conclusions

The developed co-simulation model has a great advantage over classical state space models because it has the benefits of two different software environments (which lead to interesting results). MATLAB/Simulink offers a great flexibility for control algorithms and power converters modeling while MagNet provides an easy way to analyze the induction machine's behavior because non-linear materials' characteristics and specific phenomena are taken into account.

The resulting current for the sinusoidal three-phase symmetrical voltage supply system has a RMS value of 0.55A, which is the rated value. When the six-pulse voltages supply system was used the resulting current has a RMS value of 0.69A, so is about 25% greater. This increased value is the effect of the increased RMS value of the six-pulse voltages in comparison with the sinusoidal ones (as Fig. 9 shows the same peak value was supposed for both sinusoidal and six-pulse voltages because this value is the one that stresses the motor's electrical insulation). Thus the ohmic losses are about 57% greater than their rated value. Also, as Fig. 11 depicts, the induction motor has a greater acceleration (during the start-up transient regime $t < 50$ ms – see Fig. 10) for the six-pulse voltage case, due to a greater net torque (given by the greater RMS value of the currents).

If one wants to obtain the same RMS value for exponential currents (the six-pulse voltages supplying system case) as for sinusoidal ones (the sinusoidal three-phase symmetrical voltage system case) then the output six-pulse voltage of the inverter should be lowered. Unfortunately this leads to a decrease of the RMS value of the fundamental. Another possible solution could be to place a filter at the inverter's output and so a sinusoidal voltage would be applied at the induction motor's terminals.

The magnetic flux density map shows that in case of a six-pulse voltage supply (see Fig. 13) the motor's magnetic core is more saturated than in the case of sinusoidal voltage supply (see Fig. 12). Thus the iron losses are greater than their rated value. A possible way to reduce this phenomenon would be to increase the yoke and the teeth width.

If no core modification is applied and no filter is used, then it is clear that the machine should have a better cooling system, especially if the induction motor

has an intermittent operation regime (elevators, traction drives etc.). In this case the speed is controlled by the input DC voltage of the inverter.

Based on the simulation results it was found that the six-pulse voltage supply does not generate circulating currents that would flow through the capacitive couplings between the stator and the rotor because the magnetic field's frequency is low. One of the issues that may still occur is high insulation stress of the first turns of the stator's winding due to the short rising times of the supplying voltages. In the worst case this phenomenon could lead to partial electrical discharges between these turns.

The paper can also be used as guide for teaching purposes because it presents some issues on how it is possible to model an induction machine and its supplying converter. This also proves how manufacturers use the advantage of different modeling and simulation software environments in order to create virtual prototypes.

REFERENCES

[1]. *R. Belmans*, Noise in inverter-fed squirrel-cage induction motors, Modern Electrical Drives, 2000 Kluwer Academic Publishers, Section IX.3, pp. 655-684, 2000.

[2]. *S. Van Haute, A. Malfait, R. Belmans*, Influence of switching frequency and squirrel cage design on audible noise and losses in induction motor drives, EPE Journal, **Vol. 7**, No.1-2, pp. 67-72, August-October, 1997.

[3]. *E. Persson,* Transient effects in applications on PWM inverters to induction motors, IEEE Transactions on Industrial Applications, **vol. 28**, pp. 1095 – 1101, 1992.

[4]. *N. Srb, S. Štjepan*, High-frequency oscillations in induction machine stator windings at impulse tests with and without rotor. PEMC' 96, Part 2, pp. 44-48, Budapest, 1996.

[5]. *J. Knockaert, J. Peuteman, J. Catrysse and R. Belmans*, Hidden reflection phenomena on inverter-fed induction motors, Proc. EPE 2005 Dresden (CD-ROM).

[6]. *B. De Vivo, L. Egiziano, P. Lamberti, V. Tucci*, Influence of circuit parameters on the electric discharge machining of the bearings of a PWM inverter driven motor, SPEEDAM 2008, International Symposium on Power Electronics, Electrical Drives, Automation and Motion, art. no. 4581143, pp. 1321-1324, 2008.

[7]. *L. N. Modran*, Digital simulation of induction and permanent magnet synchronous motor starting, 2008 11th International Conference on Optimization of Electrical and Electronic Equipment, OPTIM 2008, art. no. 4602513, pp. 139-146, 2008.

[8]. *S. A. Saleh, M. A. Rahman*, Real-time performance testing of a 3-phase VS WM inverter-fed induction motor, 2007 European Conference on Power Electronics and Applications, EPE, art. no. 4417232, 2007.

[9]. *S. C. Sabharwal*, Methodology for estimating performance characteristics of three phase induction motor operating direct-on-line or with six pulse inverter, 2006 International Conference on Power Electronics, Drives and Energy Systems, PEDES '06, art. no. 4147838, 2006.

[10]. *D. G. Dorrell, C. Y. Leong, R. A. McMahon*, Analysis and performance assessment of six-pulse inverter-fed three-phase and six-phase induction machines, IEEE Transactions on Industry Applications 42 (6) – 2006, pp. 1487-1495, 2006.

[11]. *O. Bottauscio, M. Chiampi, C. Concari, C. Tassoni, M. Zucca*, From the ideal to the real induction machine: Modeling approach and experimental validation, Journal of Magnetism and Magnetic Materials 320 (20) – 2008, pp. e901-e906, 2008.
[12]. *K. Hameyer, R. Belmans, R. De Weerdt, E. Tuinman*, Finite element analysis of steady state behavior of squirrel cage induction motors compared with measurements, IEEE-Transactions on Magnetics, part II, No.2, **Vol.33**, pp. 2093-2096, March, 1997.
[13]. *R. Belmans, D. Verdyck, W. Geysen, R. D. Findlay, B. Szabados, S. Spencer, S. Lie*, Magnetic field analysis in squirrel cage induction motors, IEEE Transactions on Magnetics, **Vol.28**, No.2, pp. 1367-1370, , March, 1992.
[14]. *R. De Weerdt, K. Hameyer, R. Belmans*, End winding leakage calculation of a squirrel-cage induction motor for different load conditions, COMPEL-ISEF'95 Proc., **Vol.14**, No.4, pp. 85-88, December, 1995.
[15]. *F. Henrotte, J. Heidt, E. Lange, M. Van Der Giet, K. Hameyer*, Extraction from field models of the lumped parameters of induction motors, IET Science 2008, Measurement and Technology 2 (6), pp. 447-454, 2008.
[16]. *C. Grabner*, Simplified evaluation of equivalent circuit parameters of a squirrel cage induction motor by finite element calculations and measurement, Canadian Conference on Electrical and Computer Engineering – 2008, art. no. 4564542, pp. 295-300, 2008.
[17]. *E. R. Champion, Jr. J. M. Ensminger*, Finite Element Analysis with Personal Computers, ISBN 13: 9780824779818, CRC Press, 1988.
[18]. *T. J. Hammons, H. B. Ertan, J. A. Tegopoulos, W. Drury, M. Ehsani, T. Nakata, A. G. Jack*, Highlights of the 1998 International Conference on Electrical Machines, ICEM Review, 1998.
[19]. http://www.mathworks.com.
[20]. http://www.infolytica.com.
[21]. *B. K. Bose*, Modern Power Electronics and AC Drives, Prentice Hall, Upper Saddle River, 2002.
[22]. *I. Cioc, N. Bichir, N. Cristea,* Maşini electrice – Îndrumar de proiectare, **Vol. 2**, Ed. Scrisul Românesc, Craiova, 1981.
[23]. *C. Mocanu*, Teoria câmpului electromagnetic, EDP, Bucureşti, 1981.
[24]. *D. A. Lowther, P. P. Silvester*, Computer-Aided Design in Magnetics, Springer-Verlag, 1986.
[25]. *J. Jun, C. Lee, B. Kwon*, The analysis of bearing current using common mode equivalent circuit parameters by FEM, ICEMS 2005, Proceedings of the Eighth International Conference on Electrical Machines and Systems, **Vol. 1**, pp. 49 – 51, 2005